Published in final edited form as:
ACS Nano. 2012 June 26; 6(6): 4966–4972. doi:10.1021/nn300516g.

Nuclear Mapping of Nano-Drug Delivery Systems in Dynamic Cellular Environments

Ashwinkumar A. Bhirde[1], **Ankur Kapoor**[2], **Gang Liu**[3], **Ramiro Iglesias-Bartolome**[4], **Albert Jin**[5], **Guofeng Zhang**[5], **Ruijun Xing**[1], **Seulki Lee**[1], **Richard D. Leapman**[5], **J Silvio Gutkind**[4], and **Xiaoyuan Chen**[1,*]

[1]Laboratory of Molecular Imaging and Nanomedicine, National Institute of Biomedical Imaging and Bioengineering, National Institutes of Health, Bethesda, MD 20892, USA

[2]Department of Radiology and Imaging Sciences, Clinical Center, National Institutes of Health, Bethesda, Maryland 20892.

[3]Center for Molecular imaging and translational medicine, School of Public Health, Xiamen University, Xiamen 361005 China.

[4]Oral and Pharyngeal Cancer Branch, National Institute of Dental and Craniofacial Research, National Institutes of Health, Bethesda, Maryland 20892

[5]Laboratory of Cellular Imaging and Macromolecular Biophysics, National Institute of Biomedical Imaging and Bioengineering, National Institutes of Health, Bethesda, Maryland 20982, USA

Abstract

Nanoformulations have shown great promise for delivering chemotherapeutics and hold tremendous clinical relevance. However nuclear mapping of the chemo drugs is important to predict the success of the nanoformulation. Herein in this study fluorescence microscopy and a subcellular tracking algorithm were used to map the diffusion of chemotherapeutic drugs in cancer cells. Positively charged nanoparticles efficiently carried the chemo drug across the cell membrane. The algorithm helped map free drug and drug loaded nanoparticles, revealing varying nuclear diffusion pattern of the chemotherapeutics in drug-sensitive and resistant cells in a live dynamic cellular environment. While the drug-sensitive cells showed an exponential uptake of the drug with time, resistant cells showed random and asymmetric drug distribution. Moreover nanoparticles carrying the drug remained in the perinuclear region while the drug got accumulated in the cell nuclei. The tracking approach has enabled us to predict the therapeutic success of different nanoscale formulations of doxorubicin.

Keywords

iron oxide nanoparticles; doxorubicin; drug resistance; computational; nuclear mapping; live cell imaging; cancer

Although a number of chemotherapeutic drugs are available to treat various cancers, severe toxicity and unpredictable efficacy are frequently seen with existing therapies.[1,2] In addition, significant limitations exist with chemotherapy, including inadequate dosing at the disease sites, acute and long-term drug toxicity, and possible tumor recurrence as a result of drug resistance.[3-7] To counteract these difficulties, combinations of chemotherapeutic drugs and nanomaterials,[8] have been formulated to deliver drugs at high concentrations to the sites of

*Correspondence: Xiaoyuan Chen, shawn.chen@nih.gov.

disease while maintaining lower and less toxic systemic concentrations in the patient. Various organic/inorganic, biological as well as synthetic nanomaterials are currently under investigation for these nano-drug formulations.[9-15] Enzyme and pH responsive and receptor specific nano-drug formulations are major ones being developed.[16] Among the imaging modalities PET, CT and MRI have been the most widely used and clinically implemented techniques. For molecular and functional imaging strategies used in nano-drug development bioluminescence and fluorescence imaging have evolved as important imaging tools.[17]

Chemotherapeutic drugs, e.g., cisplatin and doxorubicin, kill cancer cells by intercalating with the DNA, thereby disrupting the cell growth and division process.[18-20] However, even with advanced nano-drug formulations, the delivery of an insufficient drug concentration to the nuclei of tumor cells in the patient may lead to unsuccessful treatment.[21] Use of live cell fluorescence microscopy for imaging the subcellular distributions of drugs is critical for assessing the biological effects of chemotherapeutic formulations.[22] Recent advances in live cell imaging have included the ability to track cells automatically.[23] However, most algorithms for cellular tracking require the use of fluorescent signals originating from genetically modified proteins.[24] Here, we have developed a technique for directly tracking chemotherapeutics successfully in single cells based on the intrinsic fluorescence of the drug without using selective stains or fluorescent proteins as labels.

The nano-drug formulation that we have constructed combines the drug doxorubicin (DOX) and superparamagnetic iron oxide nanoparticles (SPIONPs). Magnetic nanocrystals like SPIONPs have been developed mainly as MRI contrast agents and as magnetic labels for tracking stem cells.[25-27] DOX is an FDA-approved drug, which is a clinically relevant chemotherapeutic for a variety of cancers, particularly ovarian cancer.[28, 29] It has been demonstrated that SPIONPs can function as drug delivery vehicles to reach tumor sites and can also be imaged through MR contrast.[30, 31, 32, 33] Although the loading of SPIONPs with chemotherapeutic drugs has recently been investigated,[34, 35] there are no reports of live imaging of the entire drug delivery system, including the drug itself in a dynamic cellular environment. We have synthesized highly aqueous, dispersed polyethyleneimine (PEI)-coated SPIONPs,[36] and loaded them with doxorubicin. Our aim is to test efficacy of the nanoparticles against drug-sensitive and drug-resistant cancer cells, as well as to characterize subcellular differences in translocation and accumulation between the free drug and the nano-drug delivery system.

RESULTS AND DISCUSSION

Synthesis and characterization of Nano-drug delivery System

Nano-drug formulation was formed by first synthesizing SPIONPs nanocrystals using branched PEI2k. DOX was loaded onto the magnetic nanocrystals and the entire drug delivery system was thoroughly characterized for size, shape, surface charge and drug loading efficiency (**Figure 1** and Supporting Information **Figure S1-S3**). The as synthesized highly aqueous dispersed PEI coated magnetic nanocrystals were characterized with transmission electron microscope (**Figure 1a)**, and atomic force microscope (**Figure 1b**) which showed a core size of ~10-15 nm and a overall size of ~50-60 nm respectively. PEI coating onto the SPIONPs was confirmed by FTIR and Zeta-potential analysis. The FTIR spectrum (Supporting Information **Figure S1**) showed the presence of amine groups on the magnetic nanoparticles at around 1400 – 1700 nm wavelength. A surface charge of 44.3 mV of the SPIONPs confirms efficient coating of the charged polymer. Fluorescence spectroscopy (Supporting Information **Figure S2**) confirmed the presence of doxorubicin (DOX) on the SPIONPs. DOX loading onto the nanoparticles was done using fluorescence analysis on a microplate reader (Supporting Information **Figure S3**). The Nanodox was

treated with diluted HCl (pH = 5) and incubated for 20 min. The DOX content was quantified at 590 nm on the microplate reader by comparing with a standard curve.

Computational Nuclear Mapping Modeling

Whereas nuclear boundaries are often clearly demarcated in microscopy of fixed cells, in live cell microscopy the boundaries are often not well defined due to the dynamically changing morphology. Furthermore, since the cells are not fixed, they may migrate away from the focal plane of the image. To take these factors into account, we have developed a semi-automated method for tracking cell nuclei in a recorded time sequence of live images. The first step in the process, shown as a flow diagram in **Figure 2a**, allows the user to pick an elliptical region that defines the nuclear boundary in the first image of a recorded time series. This region is used as a template to match the nucleus in subsequent images. To provide a similarity measure between the template (*T*) and image (*I*) a Normalized Cross Correlation (NCC) function is defined according to:

$$NCC(u,v) = \frac{\Sigma_{u,v}\left(I(x,y) - \overline{I_{u,v}}\right)\left(T(x,y) - \overline{T}\right)}{\sigma_I \sigma_T}$$

where $\bar{T}$ and $\overline{I_{u,v}}$ are mean values of the template and an image region under the template, respectively, σ_T and σ_I and are the corresponding standard deviations.

The location (u,v) in the image that maximizes NCC is considered to be the location of the elliptical region that best matched the current template. Additionally, a new elliptical region around this location replaces the current template that is then used for the next image. This process is repeated until all the images in the time series are analyzed. A log of locations of centers of elliptical regions is maintained for each of these images.

There is a possibility that NCC may not result in a correct match due to noise and ill-defined nucleus boundaries. To mitigate this scenario, we place bounds on the allowed displacement in the centers of elliptical regions between two consecutive images. The allowed displacement is determined heuristically based on the size of the elliptical region and the size of the image. If maximization of NCC fails to find a new location, the algorithm stops for a user input. A probable location based on past cell motion is presented to the user, who can adjust this location manually using a graphical user interface. The algorithm resumes by using this manually updated location for the next iteration of the NCC based algorithm (Supporting Information **Note**). Once the entire series is processed, a median filter of width 5 pixels is applied to smooth the trajectory of the elliptical region center. Finally, this elliptical region with a smooth trajectory is used as a mask to compute the distribution of drug or drug-loaded nanoparticles inside the nucleus. A simple representative snapshot of the result of the algorithm is shown in **Figure 1b** where the top panel shows optical tracking of a whole cell with marked nuclei while the bottom panel shows the fluorescent view of the whole cell and nucleus alone in a single cancer cell.

Nuclear Mapping of Nano-Chemotherapeutics in Drug-sensitive Cells

Our study involved two drug delivery systems studied in drug sensitive and drug resistant cells: the FDA approved DOX drug, adramycin and DOX-loaded SPIONPs (Nanodox). These were both tested for cell penetration and nuclear accumulation. DOX sensitive OVCAR8 cancer cells were treated with either free drug or Nanodox (Supporting Information **Videos S1-S2**). Live microcopy monitoring showed the presence of the drug in the cells as early as 25 min for the free drug and 5 min for the Nanodox (**Figure 3a** and Supporting Information **Videos S3-S4**). Cells treated with free drug and Nanodox

formulation and showing DOX accumulation were also fixed and stained for organelle localization (**Figure 1c**) 1 hr post treatment. Analysis of Z-stack images of the fixed cells showed nuclear drug uptake in drug-sensitive cells from both free drug and Nanodox. However, nuclear mapping using our tracking algorithm showed a marked difference between early uptake of the free drug and uptake of the drug loaded onto the SPIONPs (**Figure 1d**). The overall cellular uptake of the Nanodox was fivefold higher than the drug on its own in 60 min (**Figure 1e**). After washing and incubation with medium for 3 h, the presence of DOX was clearly observed in the nuclear region for both free drug and Nanodox (Supporting Information **Figure S4**). The uptake of drug into the drug-sensitive cells was exponential both in nuclear and non-nuclear cellular region. Notably the Nanodox formulation was able to take minimal dosage to the cancer cell nuclei in concentrated amount that is clinically desired.

Nuclear Mapping of Nano-Chemotherapeutics in Drug-resistant Cells

Drug-resistant OVCAR8/ADR cancer cells were treated with free DOX and Nanodox and observed live in a dynamic environment (Supporting Information **Videos S5-S6**). Nuclear mapping with the drug-resistant OVCAR8/ADR cells showed sharp contrast between the uptake of the free drug and uptake of the drug loaded onto SPIONPs (**Figure 4a** and Supporting Information **Videos S7-S8**). The overall cellular uptake of the Nanodox was almost five times greater than the drug on its own at 60 min time point. The free drug and Nanodox had similar uptake profiles for the first 30 min of treatment in the resistant cells. This behavior was quite different from that of drug-sensitive cells. After incubation with medium for 3 h, the presence of drug was still observed in 90% of the Nanodox treated cells, but was rarely seen in free DOX treated cells, as the free drug was readily effluxed from the drug-resistant cells (Supporting Information **Figure S5**). Uptake of free DOX on its own was observed only in couple of cells, which did cross the cell membrane and reached the cell nucleus. Nanodox was the most effective in crossing the cellular barrier. DOX on the SPIONPs was able to penetrate almost all the DOX resistant cancer cells with couple of cells showing nuclear uptake. Data obtained shows very high cellular penetration of the nanoformulation, which can counteract drug resistance.

Observations at longer time intervals showed similar drug uptake patterns in both free DOX and Nanodox formulations for the drug-sensitive cells, whereas uptake of Nanodox was higher than uptake of free drug in drug-resistant cells (Supporting Information **Figure S6**). These findings were further supported by cell viability assays where both OVCAR8 and OVCAR8/ADR cells treated with varying drug concentrations in free form, and nanoformulation hindered the cell growth with increasing drug concentration (**Figure 5**). Cell viability of drug-sensitive (**Figure 5a**) and resistant (**Figure 5b**) cancer cells were carried out to check the dosage dependent killing of the cells using the standard MTT assay. The absorption was measured at 570 nm using a microplate spectrofluorometer and the relative percentage of the control (untreated) cells, which were not exposed to the drug, were used to represent 100% cell viability.

Mapping of Nano-Chemo Delivery System in Dynamic Cellular Environment

It is important to determine the fate of the delivery vehicle in addition to the drug, which can be mapped by its intrinsic fluorescence. To achieve this DOX loaded nanoparticles were labeled with FITC, and cells were treated and observed live (**Figure 6a-b**, and Supporting Information **Video S9**). It was found that the drug loaded onto the SPIONPs reached the nuclear region first, whereas the nanoparticles were mostly concentrated in the cytoplasm and plasma membrane. This observation was confirmed by examining the nanoparticles alone without the drug in live microscopy (Supporting Information **Video S10**) as well as TEM (**Figure 6c**). Data analysis using the tracking algorithm showed that drug loaded onto

the nanoparticles had the highest probability of entering the cell nucleus (**Figure 6d**). Overall non-nuclear uptake of the drug loaded onto the nanoparticles was higher compared to both free drug and free particles (**Figure 6e**). The data suggest that the Nanodox formulation could provide an approach to cancer treatment irrespective of the sensitiveness of the cells to the drug. Data presented here suggest that computational mapping can lead to prediction of therapeutic results for nuclear sensitive drugs and drug delivery system. The masking technique can help elucidate drug uptake, diffusion rate and transport mechanism. The algorithm can be used for any fluorescent drug, drug tagged with a fluorescent probe or a fluorescent probe itself. This *ex vitro* image analysis can also be implemented for *ex vivo* analysis in a dynamic environment.

Conclusions

In summary, we show that a combination of live cell imaging and tracking can be used to assess variations in nuclear uptake of chemotherapeutics between drug-sensitive and drug-resistant cells. Our results suggest that positively charged magnetic nanoparticles are efficient in carrying chemotherapeutics across cell membranes, and that the drug delivered has an increased probability of entering the nucleus. Whereas in sensitive cells free drug and nanoparticle-loaded drug behaved similarly over time, resistant cancer cells appear immune to the free drug. This suggests that a quicker cell-penetrating and drug-release nanoparticle formulation acts as a camouflage in counteracting cancer cells resistant to drugs. The data presented here strongly suggest that nuclear mapping of live cells is very important in determining the successful outcome of a nanoformulation with chemotherapeutics. Moreover the computational methodology adapted in this study can be used to track specific fluorescent targets of interest in a single cell by masking less relevant regions of cells maintained in a dynamic environment.

METHODS

Synthesis of Nanodox

Nanodox was synthesized following a previously described procedure. Briefly, branched PEI2k (Alfa Aesar) was reacted with 1-iododododecane (Aldrich) in ethanol and the pure product was obtained as a gummy solid on lyophilization and confirmed by ^{1}H NMR ($CDCl_3$). $Fe(acac)_3$ (2 mmol) was mixed with 1,2-hexadecanediol (10 mmol), oleic acid (6 mmol), and oleylamine (6 mmol) in benzyl ether (20 mL) under nitrogen and heated to reflux (~300 °C) for 1 h. The product was resuspended in hexane in the presence of oleic acid and oleylamine and reprecipitated with ethanol to give SPIONPs. These nanocrystals in hexane were dried under argon and redispersed in chloroform together with alkylated PEI2k and DOX. Then, mixed solution was slowly added into water with sonication to form Nanodox. The resulting particles were collected by centrifugation and were redispersed in PBS buffer solution. The iron content was analyzed by following a previously published protocol[2]. For DOX content analysis, a small portion of the product was added to a diluted HCl solution (pH = 5) and incubated for 20 min. The solution was then subjected to fluorescence analysis on a microplate reader (Synergy 2 Multi-Mode Microplate Reader, BioTek). The readout at 590 nm was recorded and compared with a standard curve to determine the concentration.

Cell Culture

We thank Dr. Neamati at the University of Southern California for providing us the OVCAR8 and OVCAR8/ADR cells. OVCAR8 and OVCAR8/ADR cancer cells were cultured in RPMI (Invitrogen) supplemented with 10% fetal bovine serum (FBS) at 37°C in 95% air/5% CO_2. Freshly plated cells were grown overnight, to 50-70% confluency prior to incubation with nanochemo formulation for live imaging.

FTIR of Nano-drug formulation

Fourier transform infrared spectroscopy (FTIR) of Nanodox along with controls Alkyl-PEI2k-SPIONPs and DOX alone was done using KBr pellets of each. The wave numbers of the transmittance of each sample were recorded using a PerkinElmer spectrum GX spectrophotometer.

Fluorescence Spectrometry

Fluorescence spectrometer analysis was carried out on DOX loaded Alkyl-PEI2k-SPIONPs and FITC conjugated Alkyl-PEI2k-SPIONPs. For this fluorescence spectra of Alkyl-PEI2k-SPIONPs-FITC and Alkyl-PEI2k-SPIONPs-DOX nano-chemo formulation along with free DOX and FITC alone as controls were carried-out using a Perkin-Elmer LS55 fluorescence spectrometer (Perkin-Elmer).

Atomic Force Microscope analysis of Alkyl-PEI2k-IONP

Tapping mode AFM studies were performed on a PicoForce Multimode platform with a Nanoscope V controller (Bruker, Santa Barbara, CA), using a type E scanner head with a FESP type of cantilever, on a mica substrate, and following standard optimizations.

Zeta Potential

To find the surface charge of the nanoparticles, zeta potential analysis was carried-out using a Zetasizer Nano series (Zen3600) from Malvern with zetasizer software 6.0 as the interface.

Confocal Fluorescence Microscopy

DOX sensitive and resistant cancer cells were grown into 50-60% confluency on 8-well chambered LabTek II coverglass, treated with either free drug DOX, Alkyl-PEI2k-SPIONPs-FITC, Nanodox or DOX loaded and FITC labeled Alkyl-PEI2k-SPIONPs nano-chemo formulation and, live cell time series imaging or z-stack intercellular uptake analysis was carried out for 1 hr. Live cell imaging was performed using an inverted Zeiss LSM 700 confocal microscope equipped with CO_2 module, heating unit and heating plate using a 40x/0.75 M27 EC Plan-Neofluar objective. Imaging was carried out at 37°C in 5% CO_2 with cells plated in LabTek II coverglass. Images were acquired and processed with the Zeiss Zen 2009 image software. The fluorescence micrographs shown are representative of at least three independent experiments. Average fluorescence intensity was quantified using Zen 2009 software.

Transmission Electron Microscope imaging of Magnetic Nanocrystals

A specimen of PEI coated SPIONPs for TEM imaging was carried out by depositing a 3 μL droplet from the aqueous solution onto a Quantifoil grid and left to dry in air. After adsorption for 3 min, the excess solution was blotted with filter paper, washed with a few 3-μL droplets of de-ionized water in order to remove any dirt, and left to dry. Images were recorded in a Tecnai TF30 TEM (FEI, Hillsboro, OR, USA) equipped with a Gatan Ultrascan 1000 CCD camera (Gatan, Pleasaton, CA, USA).

Cell Proliferation (MTT) assay

Cells were grown to 50-70% confluency overnight in 96 well plates. Next, the medium was aspirated and the cells incubated with fresh medium containing either free nanoparticles and drug alone or nano-chemo formulation for 48 h. Post treatment, the cells were washed 2x with PBS, cells were incubated for an additional 24 h in fresh medium. MTT was assessed using the CellTiter 96 AQ One Solution Cell Proliferation Assay kit (Promega, WI), and measured optically at 570 nm using a microplate spectrofluorometer.

Supplementary Material

Refer to Web version on PubMed Central for supplementary material.

Acknowledgments

This research was supported by the intramural programs of the National Institute of Biomedical Imaging and Bioengineering, NIH.

References

1. Zahedi P, De Souza R, Piquette-Miller M. Optimizing Cancer Care: Is the Future Bright? Clin. Pharmacol. Ther. 2011; 90:347–350. [PubMed: 21862960]
2. Lameire N, Kruse V, Rottey S. Nephrotoxicity of Anticancer Drugs--an Underestimated Problem? Acta. Clin. Belg. 2011; 66:337–345. [PubMed: 22145268]
3. Nielsen D, Maare C, Skovsgaard T. Cellular Resistance to Anthracyclines. Gen. Pharmacol. 1996; 27:251–255.
4. Pachman DR, Barton DL, Watson JC, Loprinzi CL. Chemotherapy-Induced Peripheral Neuropathy: Prevention and Treatment. Clin. Pharmacol. Ther. 2011; 90:377–387. [PubMed: 21814197]
5. Fardell JE, Vardy J, Johnston IN, Winocur G. Chemotherapy and Cognitive Impairment: Treatment Options. Clin. Pharmacol. Ther. 2011; 90:366–376. [PubMed: 21814191]
6. Bergman PJ. Mechanisms of Anticancer Drug Resistance. Vet. Clin. North Am. Small Anim. Pract. 2003; 33:651–667. [PubMed: 12852241]
7. Weis SM, Cheresh DA. Tumor Angiogenesis: Molecular Pathways and Therapeutic Targets. Nat. Med. 2011; 17:1359–1370. [PubMed: 22064426]
8. Davis ME, Chen ZG, Shin DM. Nanoparticle Therapeutics: An Emerging Treatment Modality for Cancer. Nat. Rev. Drug Discov. 2008; 7:771–782. [PubMed: 18758474]
9. Bhirde AA, Patel S, Sousa AA, Patel V, Molinolo AA, Ji Y, Leapman RD, Gutkind JS, Rusling JF. Distribution and Clearance of PEG-Single-Walled Carbon Nanotube Cancer Drug Delivery Vehicles in Mice. Nanomedicine (Lond). 2010; 5:1535–1546. [PubMed: 21143032]
10. Yan Y, Ochs CJ, Such GK, Heath JK, Nice EC, Caruso F. Bypassing Multidrug Resistance in Cancer Cells with Biodegradable Polymer Capsules. Adv. Mater. 2010; 22:5398–5403. [PubMed: 20976679]
11. Meng H, Liong M, Xia T, Li Z, Ji Z, Zink JI, Nel AE. Engineered Design of Mesoporous Silica Nanoparticles to Deliver Doxorubicin and P-glycoprotein siRNA to Overcome Drug Resistance in a Cancer Cell Line. ACS Nano. 2010; 4:4539–4550. [PubMed: 20731437]
12. Sengupta S, Eavarone D, Capila I, Zhao G, Watson N, Kiziltepe T, Sasisekharan R. Temporal Targeting of Tumour Cells and Neovasculature with a Nanoscale Delivery System. Nature. 2005; 436:568–572. [PubMed: 16049491]
13. Ma XW, Zhao YL, Liang XJ. Nanodiamond Delivery Circumvents Tumor Resistance to Doxorubicin. Acta. Pharmacol. Sin. 2011; 32:543–544. [PubMed: 21532613]
14. Chow EK, Zhang XQ, Chen M, Lam R, Robinson E, Huang H, Schaffer D, Osawa E, Goga A, Ho D. Nanodiamond Therapeutic Delivery Agents Mediate Enhanced Chemoresistant Tumor Treatment. Sci. Transl. Med. 2011; 3:73ra21.
15. Bhirde AA, Patel V, Gavard J, Zhang G, Sousa AA, Masedunskas A, Leapman RD, Weigert R, Gutkind JS, Rusling JF. Targeted Killing of Cancer Cells *In Vivo* and *In Vitro* with EGF-Directed Carbon Nanotube-Based Drug Delivery. ACS Nano. 2009; 3:307–316. [PubMed: 19236065]
16. Koo H, Huh MS, Sun IC, Yuk SH, Choi K, Kim K, Kwon IC. *In Vivo* Targeted Delivery of Nanoparticles for Theranosis. Acc. Chem. Res. 2011; 44:1018–1028. [PubMed: 21851104]
17. Willmann JK, van Bruggen N, Dinkelborg LM, Gambhir SS. Molecular Imaging in Drug Development. Nat. Rev. Drug Discov. 2008; 7:591–607. [PubMed: 18591980]
18. de Jongh FE, van Veen RN, Veltman SJ, de Wit R, van der Burg ME, van den Bent MJ, Planting AS, Graveland WJ, Stoter G, Verweij J. Weekly High-Dose Cisplatin is a Feasible Treatment

Option: Analysis on Prognostic Factors for Toxicity in 400 Patients. Br. J. Cancer. 2003; 88:1199–1206. [PubMed: 12698184]

19. Fornari FA, Randolph JK, Yalowich JC, Ritke MK, Gewirtz DA. Interference by Doxorubicin with DNA Unwinding in MCF-7 Breast Tumor Cells. Mol. Pharmacol. 1994; 45:649–656. [PubMed: 8183243]
20. Momparler RL, Karon M, Siegel SE, Avila F. Effect of Adriamycin on DNA, RNA, and Protein Synthesis in Cell-Free Systems and Intact Cells. Cancer Res. 1976; 36:2891–2895. [PubMed: 1277199]
21. Zeller C, Dai W, Steele NL, Siddiq A, Walley AJ, Wilhelm-Benartzi CS, Rizzo S, van der Zee A, Plumb JA, Brown R. Candidate DNA Methylation Drivers of Acquired Cisplatin Resistance in Ovarian Cancer Identified by Methylome and Expression Profiling. Oncogene. Jan 16.2012 doi: 10.1038/onc.2011.611.
22. Torchilin VP. Fluorescence Microscopy to Follow the Targeting of Liposomes and Micelles to Cells and Their Intracellular Fate. Adv. Drug Deliv. Rev. 2005; 57:95–109. [PubMed: 15518923]
23. Hamilton N. Quantification and Its Applications in Fluorescent Microscopy Imaging. Traffic. 2009; 10:951–961. [PubMed: 19500318]
24. Muzzey D, van Oudenaarden A. Quantitative Time-Lapse Fluorescence Microscopy in Single Cells. Annu. Rev. Cell Dev. Biol. 2009; 25:301–327. [PubMed: 19575655]
25. Mikhaylov G, Mikac U, Magaeva AA, Itin VI, Naiden EP, Psakhye I, Babes L, Reinheckel T, Peters C, Zeiser R, Bogyo M, Turk V, Psakhye SG, Turk B, Vasiljeva O. Ferri-Liposomes as an MRI-Visible Drug-Delivery System for Targeting Tumours and Their Microenvironment. Nat. Nanotechnol. 2011; 6:594–602. [PubMed: 21822252]
26. Namiki Y, Namiki T, Yoshida H, Ishii Y, Tsubota A, Koido S, Nariai K, Mitsunaga M, Yanagisawa S, Kashiwagi H, Mabashi Y, Yumoto Y, Hoshina S, Fujise K, Tada N. A Novel Magnetic Crystal-Lipid Nanostructure for Magnetically Guided *In Vivo* Gene Delivery. Nat. Nanotechnol. 2009; 4:598–606. [PubMed: 19734934]
27. Plank C. Nanomedicine: Silence the Target. Nat. Nanotechnol. 2009; 4:544–545. [PubMed: 19734920]
28. Paoloni M, Khanna C. Translation of New Cancer Treatments from Pet Dogs to Humans. Nat. Rev. Cancer. 2008; 8:147–156. [PubMed: 18202698]
29. Otterson GA, Villalona-Calero MA, Sharma S, Kris MG, Imondi A, Gerber M, White DA, Ratain MJ, Schiller JH, Sandler A, Kraut M, Mani S, Murren JR. Phase I Study of Inhaled Doxorubicin for Patients with Metastatic Tumors to the Lungs. Clin. Cancer Res. 2007; 13:1246–1252. [PubMed: 17317836]
30. Bhirde A, Guo N, Chen X. Targeted Nanoprobes Reveal Early Time Point Kinetics *In Vivo* by Time-Resolved MRI. Theranostics. 2011; 1:274–276. [PubMed: 21562633]
31. Weinstein JS, Varallyay CG, Dosa E, Gahramanov S, Hamilton B, Rooney WD, Muldoon LL, Neuwelt EA. Superparamagnetic Iron Oxide Nanoparticles: Diagnostic Magnetic Resonance Imaging and Potential Therapeutic Applications in Neurooncology and Central Nervous System Inflammatory Pathologies, a Review. J. Cereb. Blood Flow Metab. 2010; 30:15–35. [PubMed: 19756021]
32. Xie J, Jon S. Magnetic Nanoparticle-Based Theranostics. Theranostics. 2012; 2:122–124. [PubMed: 22287992]
33. Quan Q, Xie J, Gao H, Yang M, Zhang F, Liu G, Lin X, Wang A, Eden HS, Lee S, Zhang G, Chen X. HSA Coated Iron Oxide Nanoparticles as Drug Delivery Vehicles for Cancer Therapy. Mol. Pharm. 2011; 8:1669–1676. [PubMed: 21838321]
34. Brule S, Levy M, Wilhelm C, Letourneur D, Gazeau F, Menager C, Le Visage C. Doxorubicin Release Triggered by Alginate Embedded Magnetic Nanoheaters: a Combined Therapy. Adv. Mater. 2011; 23:787–790. [PubMed: 21287643]
35. Kievit FM, Wang FY, Fang C, Mok H, Wang K, Silber JR, Ellenbogen RG, Zhang M. Doxorubicin Loaded Iron Oxide Nanoparticles Overcome Multidrug Resistance in Cancer *In Vitro*. J. Control. Release. 2011; 152:76–83. [PubMed: 21277920]
36. Duwez AS, Cuenot S, Jerome C, Gabriel S, Jerome R, Rapino S, Zerbetto F. Mechanochemistry: Targeted Delivery of Single Molecules. Nat. Nanotechnol. 2006; 1:122–125. [PubMed: 18654163]

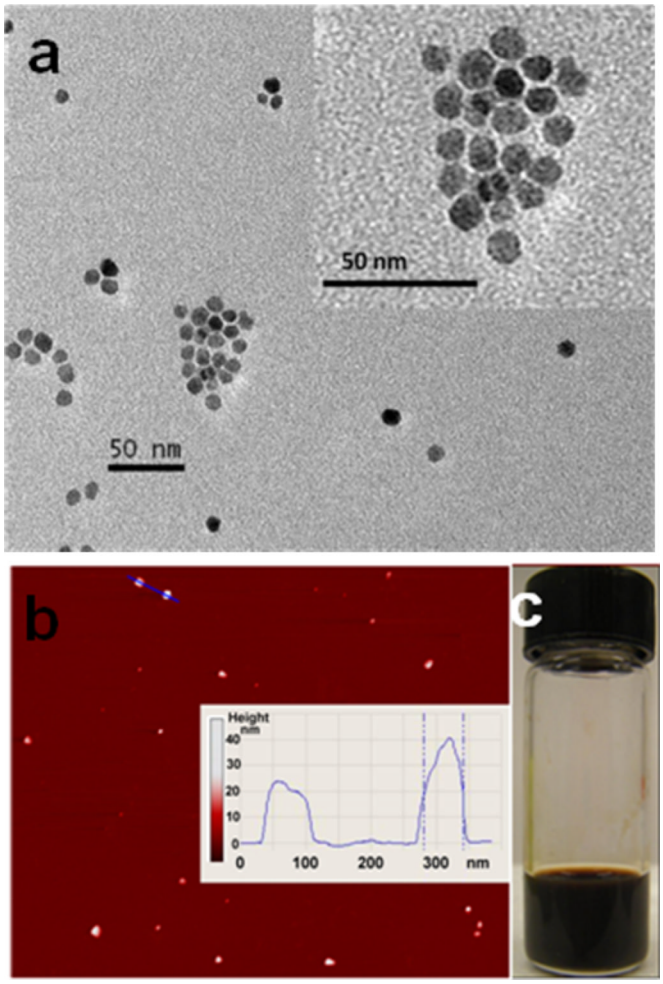

Figure 1. Electron and force microscopy characterization of nano-drug delivery vehicles

a, Transmission electron microscope (TEM) characterization of Alkyl-PEI2k-SPIONPs. TEM was used to characterize the shape and size of the material core. TEM analysis showed 10-15 nm spherical magnetic nanocyrstals. **b**, Atomic force microscope (AFM) and surface charge analysis of the Alkyl-PEI2k-SPIONPs. AFM characterization gave the hydrodynamic size of the NPs which was greater than 15 nm and less spherical than observed from TEM confirming the polymer coating. Picture showing, highly aqueous dispersed iron oxide nanoparticles with zeta-potential analysis showing a high positive charge of 44.3 mV on the nanoparticles.

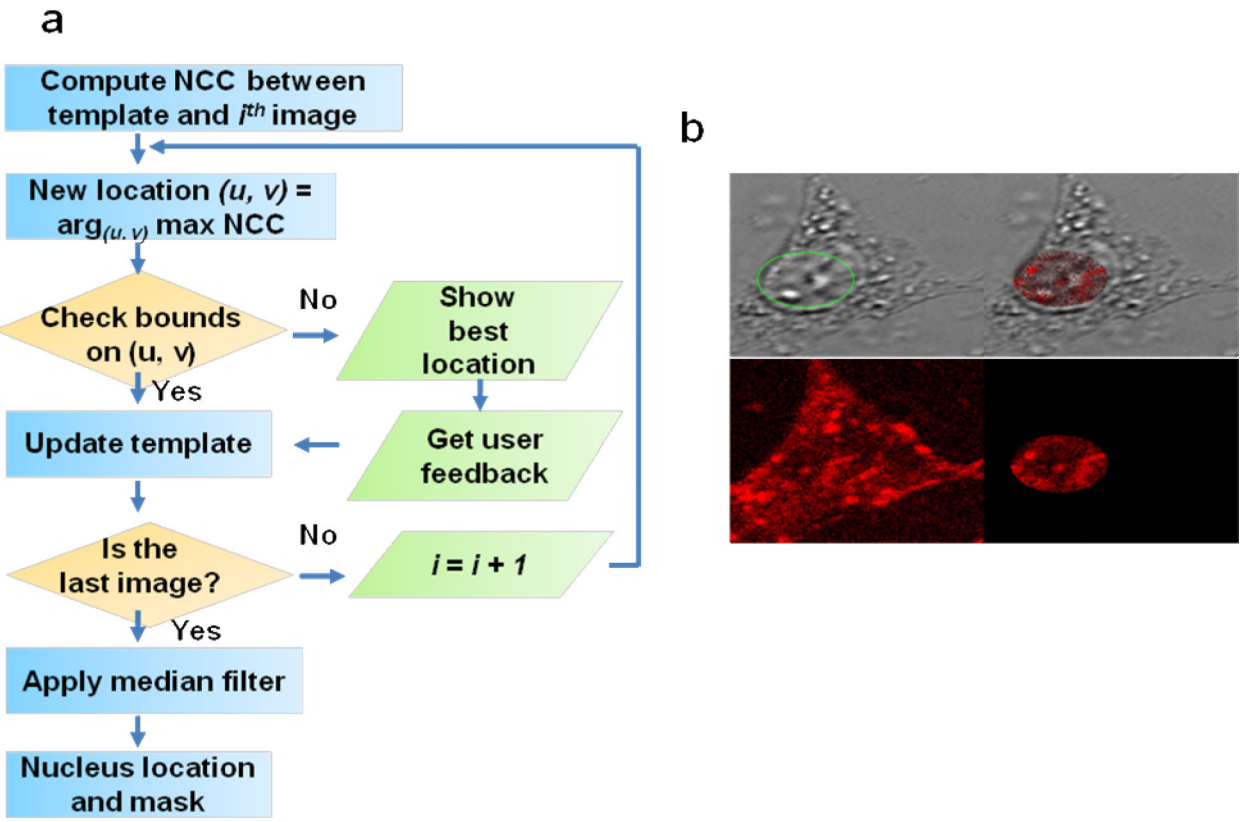

Figure 2. Flow chart for computational nucleus tracking and representative nuclear mapping of DOX in a dynamic cellular environment in cancer cells

a, The flow chart for tracking and mapping in live microscopy images shows the outline of the algorithm to obtain the location and mask of the nucleus in live imaging. The location and mask are updated for each new time point in the live image and used to compute the drug accumulation using the corresponding fluorescent channels. **b**, Screen capture of the output of the algorithm where, the top left image shows the superposition of the nucleus boundary on optical image at a given time point. The bottom left shows the corresponding DOX channel at the same time point. The bottom right shows the DOX channel intensity after applying the nucleus location and mask computed by the algorithm. After application of this mask, the image shows only intensity that is contained inside the nucleus. Since location and mask are updated continuously, the fluorescent channel intensity shown corresponds to the location of the nucleus in the current image. The top right image is the fusion of optical image and the bottom right image.

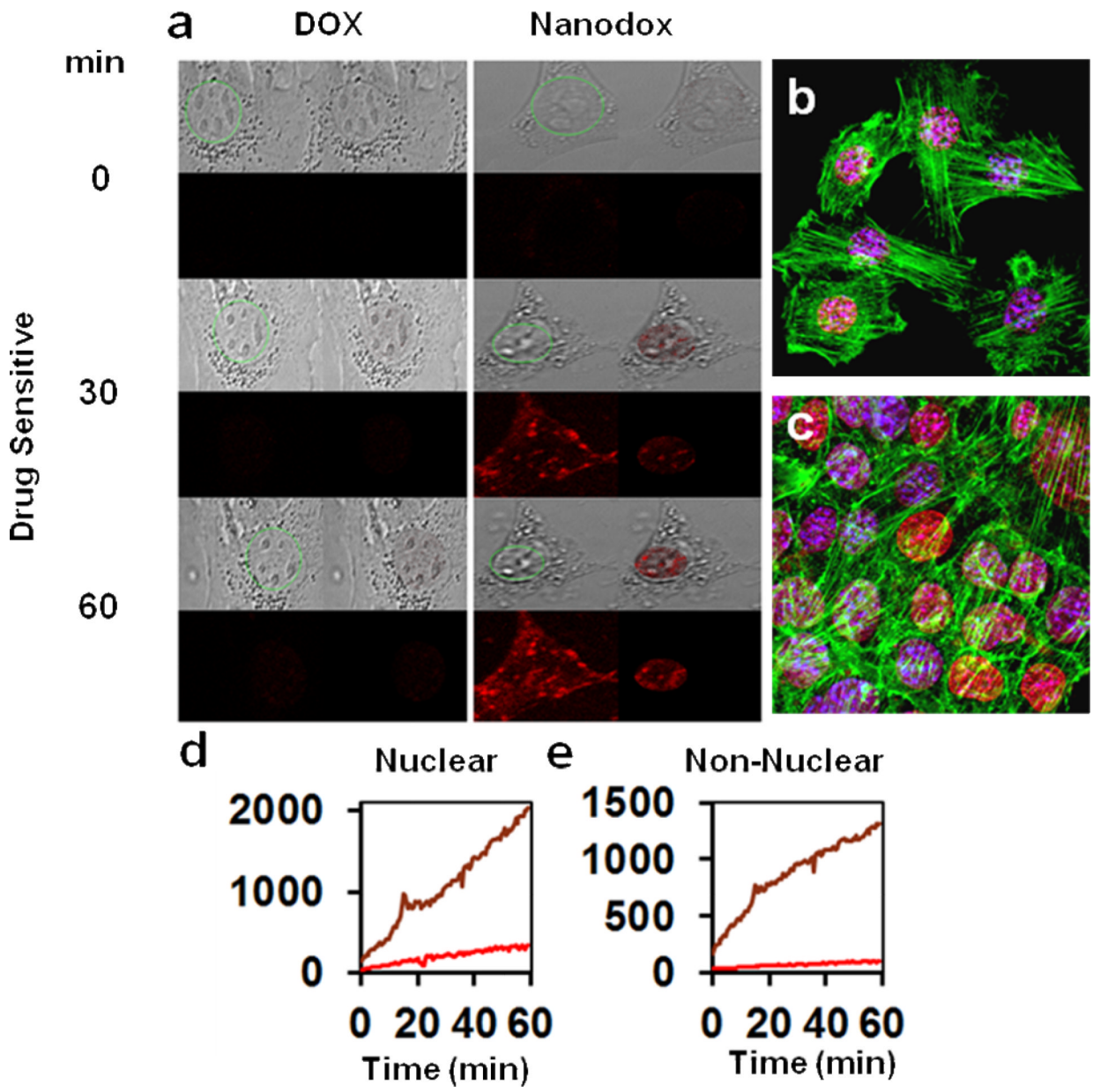

Figure 3. Representative nuclear mapping of DOX in a dynamic cellular environment

a, OVCAR8 (drug-sensitive) cells treated with free drug and Nanodox at 0, 30 and 60 min. **b**, Fixed cell images of drug-sensitive treated with free drug and Nanodox and fixed post 1 hr treatment. Cell nuclei are stained in blue and actin stained in green while the drug is in red. Both free drug and Nanodox show nuclear accumulation. Free drug shows hardly any drug accumulation and Nanodox show nuclear accumulation to some extent. **d-e**, Plot shows nuclear and non-nuclear intensity of DOX with time in the drug-sensitive cancer cells. Exponential uptake pattern is observed with both free drug and Nanodox in drug-sensitive cells. Nanodox shows significantly higher drug uptake than free DOX ($p < 0.01$). Most importantly nuclear accumulation of DOX is higher compared to non-nuclear regions for Nanodox.

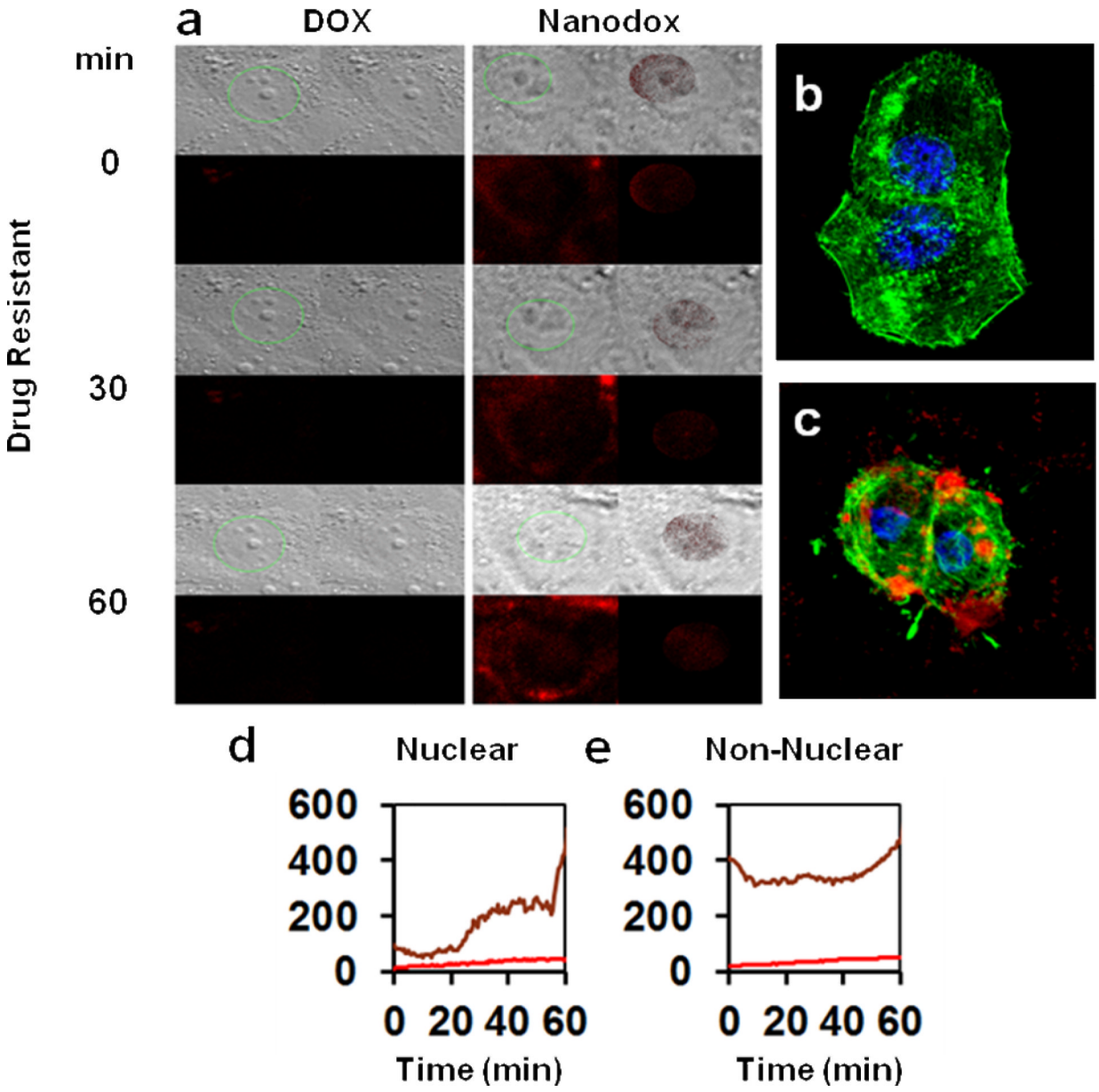

Figure 4. Nuclear mapping of DOX in resistant cancer cells in a dynamic cellular environment

OVCAR8/ADR (drug-resistant) cells treated with free drug and Nanodox at 0, 30 and 60 min. **c**, Fixed cell images of drug-resistant cells treated with free drug and Nanodox and fixed post 1 hr treatment. Cell nuclei are stained in blue and actin stained in green while the drug is in red. Both free drug and Nanodox show nuclear accumulation. Free drug shows hardly any drug accumulation and Nanodox show nuclear accumulation to some extent. **d-e**, Plot shows nuclear and non-nuclear intensity of DOX with time in the drug-sensitive cancer cells. Plot shows nuclear and non-nuclear intensity of DOX with time in the drug-resistant cancer cells. Drug uptake pattern in the drug-resistant cells is entirely different from that in the drug-sensitive cells for both free DOX and Nanodox. Nanodox shows a sudden burst of drug uptake in the nuclear region after 30 min while there is no appreciable free drug uptake in the cell nuclei.

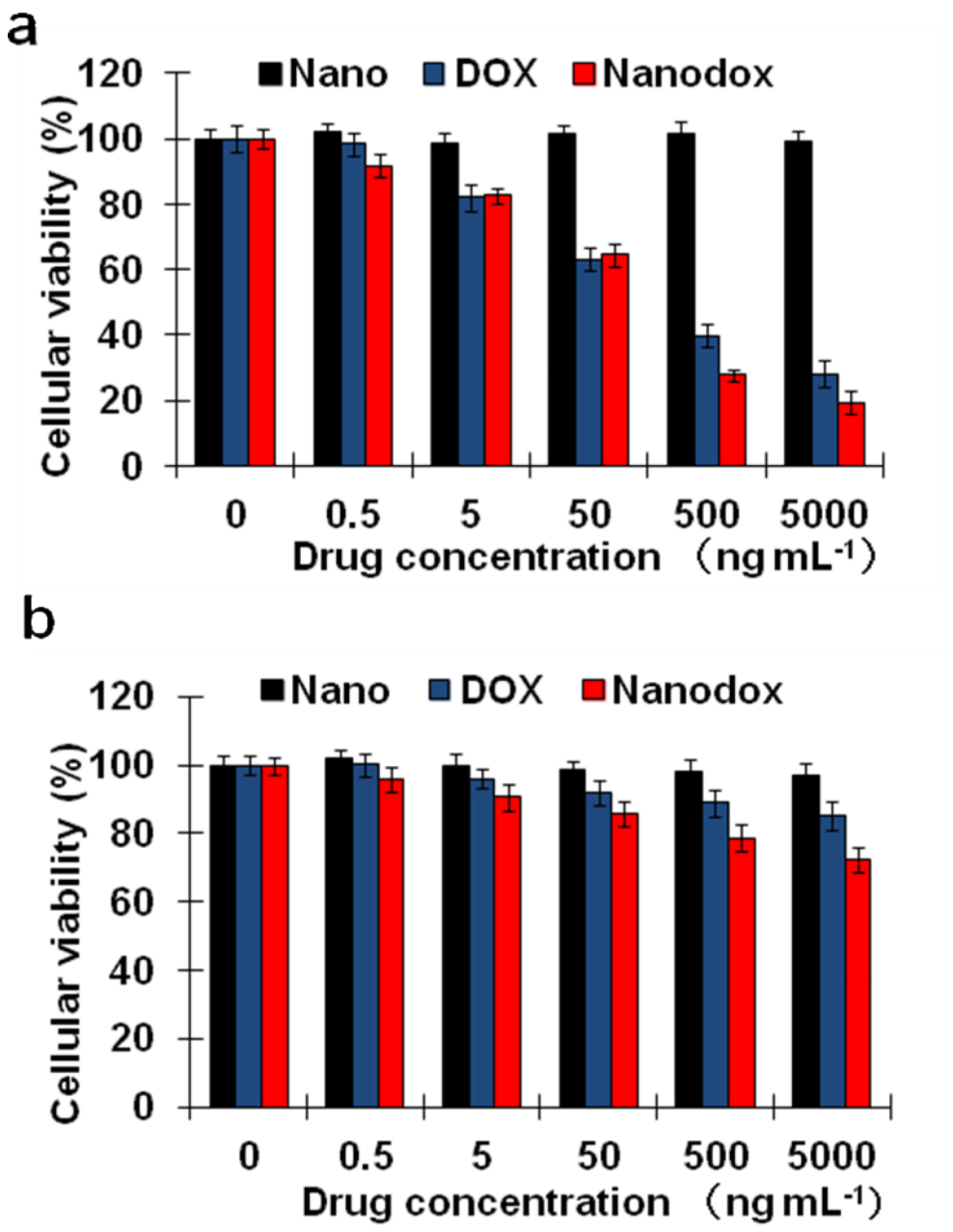

Figure 5. Cell proliferation (MTT) assay

Cell viability assay was carried out to assess the toxicity of the drug to nanoparticle in different ratios in both drug-sensitive and resistant cells. **a**, Drug-sensitive OVACAR8 and **b** drug-resistant OVACR8/ADR cells treated with nano-drug formulation for 48 hrs. The absorption was measured at 570 nm and the relative percentage of the control (untreated) cells, which were not exposed to the drug, were used to represent 100% cell viability. Nanodox showed higher toxicity to the cancer cells compared to free drug and drug free nanoparticle did not hinder the cell growth in both the cell types.

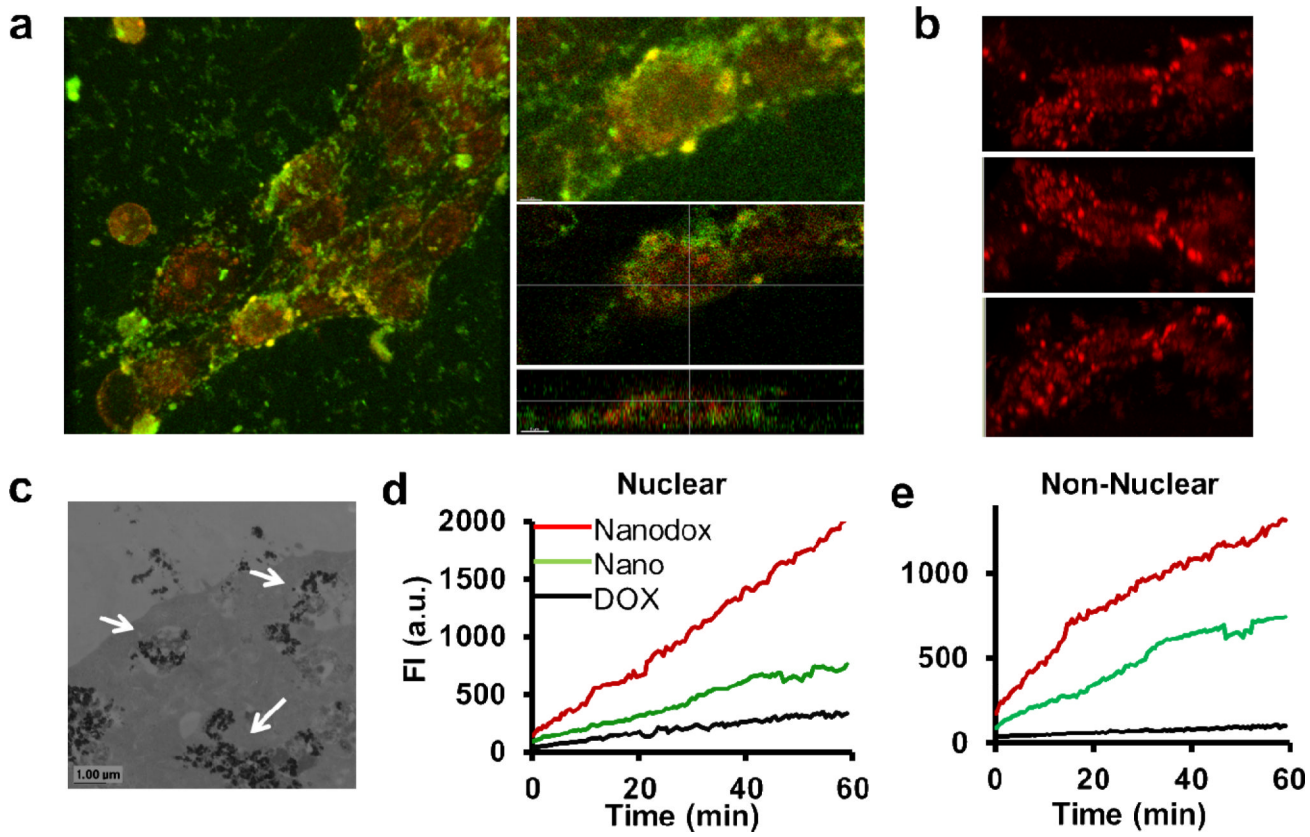

Figure 6. Nuclear mapping of Nano-drug system in a dynamic cellular environment

a, Live cell snapshots of drug-sensitive cells treated with Nanodox labeled with FITC. Drug DOX is in red, nanoparticles are in green. Nanoparticles mostly remain in the cytoplasm while majority of the drug is in the nuclear region. **b**, Z-images of Nanodox showing the cellular uptake of DOX. **c**, Direct imaging of nanoparticles using TEM. Arrows indicate nanoparticles in the cytoplasm of the cancer cell. **d**, Plot shows nuclear and non-nuclear uptake of free DOX, Nanodox and nano (FITC-labeled SPIONPs). Uptake pattern is exponential both in nuclear and non-nuclear regions. DOX loaded on the nanoparticles has the highest rate of reaching the nucleus compared to free DOX.